ENVIRONMENTAL RESEARCH
LETTERS

PURPOSE-LED PUBLISHING™

LETTER • OPEN ACCESS

Modulation of the interdecadal trend of global surface air temperature by sea surface temperature over multiple ocean basins

To cite this article: Yidan Xu *et al* 2025 *Environ. Res. Lett.* **20** 044010

ENVIRONMENTAL RESEARCH
LETTERS

OPEN ACCESS

RECEIVED
26 December 2024

REVISED
13 February 2025

ACCEPTED FOR PUBLICATION
6 March 2025

PUBLISHED
14 March 2025

LETTER

Modulation of the interdecadal trend of global surface air temperature by sea surface temperature over multiple ocean basins

Yidan Xu[1], Jianping Li[2,3,*], Jiaxu Guo[4], Jing Sun[1], Shuai Deng[1], Haohuan Fu[5,6], Lanning Wang[7] and Wei Xue[8]

[1] National Meteorological Information Centre (CMA Meteorological Data Centre), Beijing, People's Republic of China
[2] Frontiers Science Center for Deep Ocean Multi-spheres and Earth System (DOMES)/Key Laboratory of Physical Oceanography/Academy of Future Ocean/College of Oceanic and Atmospheric Sciences/ Center for Ocean Carbon Neutrality, Ocean University of China, Qingdao, People's Republic of China
[3] Laoshan Laboratory, Qingdao, People's Republic of China
[4] School of Computer Science, Shenyang Aerospace University, Shenyang, People's Republic of China
[5] Department of Earth System Science, Tsinghua University, Beijing, People's Republic of China
[6] Institute of Data and Information, Tsinghua Shenzhen International Graduate School, Shenzhen, People's Republic of China
[7] Faculty of Geographical Science, Beijing Normal University, Beijing, People's Republic of China
[8] Department of Computer Science and Technology, Tsinghua University, Beijing, People's Republic of China
[*] Author to whom any correspondence should be addressed.

E-mail: ljp@ouc.edu.cn

Keywords: global surface air temperature, interdecadal trend, multiple ocean basins, sea surface temperature, numerical simulation

Supplementary material for this article is available online

Abstract

Since the 20th century, accompanied by a long-term warming trend, the global surface air temperature (SAT) has exhibited distinct interdecadal oscillations. The period from 1910 to 2012 can be divided into four phases, including two rapid warming (1910–1945 and 1975–1998) and two warming slowdown (1940–1975 and 1998–2012) periods. This study explores the spatiotemporal characteristics of the interdecadal trends in global SAT under the influence of sea surface temperature (SST) on a multi-basin scale. Here, we have accumulated the numerical simulated SAT anomalies under the forcing of historical SST in the selected ocean basins. The results indicate that multi-basin SSTs collectively govern the spatiotemporal variations and interdecadal trends of SATs during rapid warming periods. SSTs in the Indian Ocean, North Atlantic, and western Pacific can affect the spatiotemporal interdecadal trends of SAT during 1940–1975. SSTs in the eastern tropical Pacific and North Pacific can modify the SAT spatiotemporal trends during 1998–2012. Considering the nonlinear interactions between different oceanic regions, the SAT forced by the collective SSTs in the six ocean basins shows high consistency with observation. This indicates that the combined effects of SSTs in the six ocean basins are key reasons for global SAT interdecadal change in 1910–2012.

1. Introduction

Global surface air temperature (SAT) warming exerts profound impacts on the climate system, including intensified heatwaves, altered precipitation patterns, and accelerated polar ice loss (Screen and Simmonds 2010, Dai 2013, Diffenbaugh *et al* 2017, Nie *et al* 2024, Yu *et al* 2024). These changes further cascade into socioeconomic risks, such as reduced agricultural yields, increased energy consumption, altered gross primary production growth, and heightened public health challenges (Lobell *et al* 2011, Auffhammer and Mansur 2014, Gasparrini *et al* 2015, Zhang *et al* 2024a, Zhang *et al* 2024b). Despite these well-documented consequences, driving factors influencing SAT variability, remain inadequately understood. Especially global SAT showed significant interdecadal variations alongside a long-term warming trend during 1910–2012, posing challenges for long-term climate projections and adaptation strategies.

Related works have highlighted the essential role of internal variability within the climate system in driving these interdecadal changes in SAT, in contrast to external factors such as radiative forcing (Lean and Rind 2009, Merrifield *et al* 2012, Trenberth and Fasullo 2013, England *et al* 2014, Fyfe and Gillett 2014, Dai *et al* 2015, Tan *et al* 2021). Several studies have demonstrated that processes such as ocean heat uptake, heat redistribution, dynamic atmospheric teleconnections, and interactions among different ocean basins significantly affect global SAT (Kosaka and Xie 2016, Chen and Tung 2018, Li *et al* 2018). Among the drivers of SAT variability, sea surface temperature (SST) anomalies have emerged as critical modulators of interdecadal trends.

Previous studies indicated that changes in SST in the equatorial eastern Pacific, driven by equatorial trade winds, ocean-atmosphere interactions, equatorial subsurface currents, and the Walker circulation, ultimately play a crucial role in modulating the interdecadal SAT changes (Meehl *et al* 2011, Kosaka and Xie 2013, Trenberth 2015). Additionally, the trade winds and Walker circulation drive interdecadal SST variations in the Pacific via transoceanic processes originating from the Indian Ocean. This enhanced interdecadal SST trend in the Indian Ocean ultimately leads to cooling of SST in the equatorial eastern Pacific (Timmermann *et al* 2010, Mochizuki *et al* 2016). Similarly, the Atlantic Ocean SST plays a significant role in global interdecadal SAT trend. Li *et al* (2013) found that changes in Northern Hemisphere from 1900 to 2013 was closely related to North Atlantic SST changes. The weakening of the Atlantic Meridional Overturning Circulation (AMOC) and increased heat absorption in the deep Atlantic are associated with periods of reduced global SAT warming (Keenlyside *et al* 2008, Li *et al* 2013, Chen and Tung 2014, Sun *et al* 2017, Xie and Kosaka 2017). Therefore, both the Atlantic and Indian Oceans influence global interdecadal SAT changes, either directly or through their interactions with different ocean basins (Deser *et al* 2010, Nidheesh *et al* 2013, Clement and DiNezio 2014, McGregor *et al* 2014, Nieves *et al* 2015, Sun *et al* 2015, Li *et al* 2016). Research also indicates that the influence of SST forcing from various ocean basins on interdecadal SAT trends varies across different periods (Xu *et al* 2020, 2022).

Despite significant advances in understanding SAT variability, the synergistic effects of multi-basin SST anomalies on SAT trends, particularly across distinct warming and slowdown phases, remain poorly quantified. This study builds upon prior work by conducting targeted multi-basin SST forcing experiments, systematically disentangling how basin-specific and collective SST interactions govern the spatiotemporal patterns of global SAT. By isolating contributions from key oceanic regions, we quantify the relative roles of multi-basin SSTs in driving observed interdecadal SAT variability from 1910 to 2012. Our approach bridges the gap between single-basin analyses and holistic climate system dynamics, offering new insights into the mechanisms underlying global SAT trends.

2. Data and methodology

2.1. Datasets

This study utilizes the Global SAT monthly average data from NASA's Goddard Institute for Space Studies (GISS), known as GISSTEMP. This data covers the period from 1910 to 2012 with a horizontal spatial resolution of $2^\circ \times 2^\circ$ for global grid points (Hansen *et al* 2010). The time-varying SST input data for the numerical simulations are sourced from the extended reconstructed SST version 5 (Rayner *et al* 2003) and the Hadley Center's HadISST dataset (Huang *et al* 2017), which have horizontal spatial resolutions of $2^\circ \times 2^\circ$ and $1^\circ \times 1^\circ$, respectively.

2.2. Model simulations

This study conducts sensitivity analysis experiments using the atmospheric component of the Community Earth System Model version 1.2.2, the Community Atmosphere Model version 5.3 (CAM5.3; Hurrell *et al* 2013). CAM5.3 simulations at $2^\circ \times 2^\circ$ resolution incorporate active land and thermodynamics-only sea ice components, with external forcing from 1850–2012 under historical and RCP4.5 scenarios (section S1). In the simulation experiments, the time-varying SST forces the specified ocean, while the climatological SSTs were used for other regions to isolate the role of basin-specific SST variability on global SAT trends. The model uses default parameterizations for physical processes, such as convections and cloud microphysics. The model produced monthly air temperature data from 1850 to 2012.

Model validation shows strong agreement with observed SAT trends (1910–2013) in spatiotemporal domain, with a global time series correlation coefficient greater than 0.96 and a root-mean-square error less than 0.10 °C (Xu *et al* 2020). This supports the model's utility for isolating SST-driven variability. While the model captures observed global SAT trends well, uncertainties arise from unresolved small-scale ocean-atmosphere interactions and the exclusion of dynamic ocean feedbacks in the data ocean setup. These limitations are mitigated by focusing on large-scale SST-forced variability.

This study includes eight sets of numerical simulation experiments. One set simulates global SST forcing using historical SST variations as model input. Another six sets use time-varying SST for specified oceanic regions as forcing input, while the SST for other regions remains climatological. In section 3.1, we accumulate the SAT simulated by different ocean SST forcing experiments to explore the global SAT

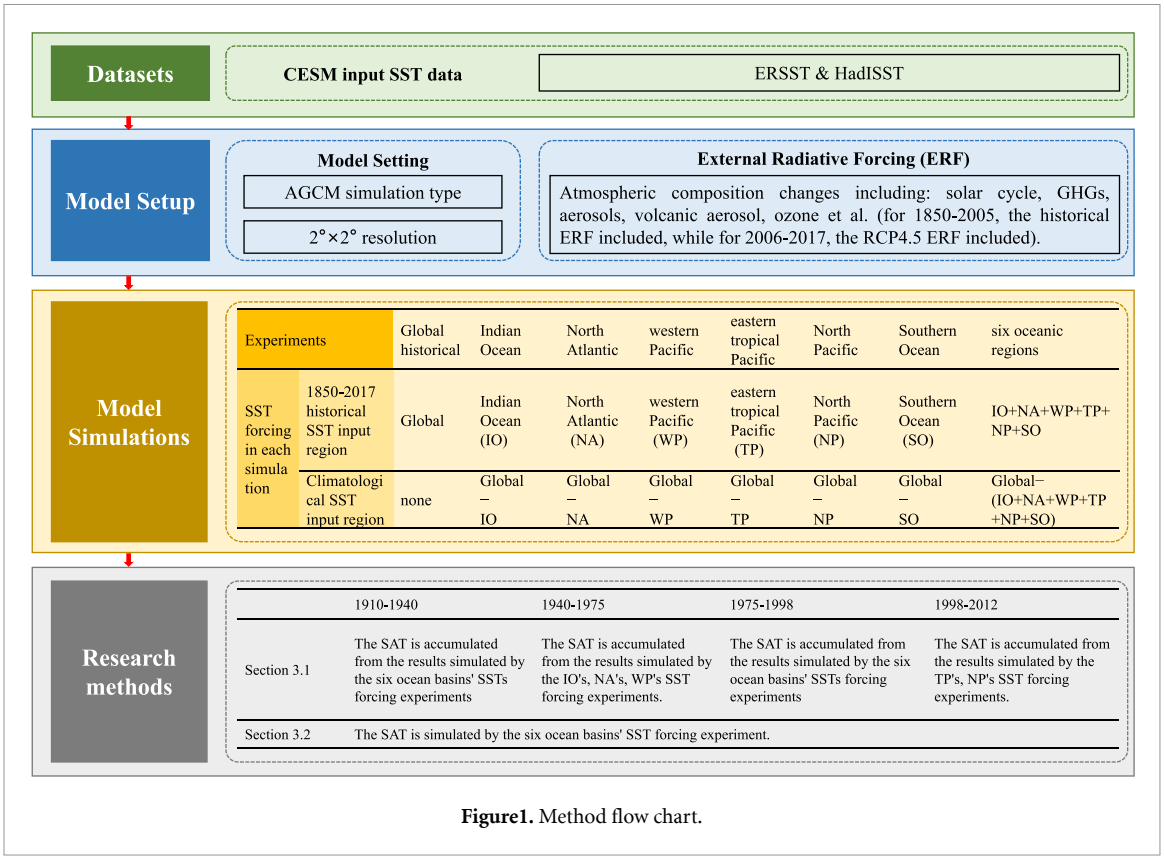

Figure1. Method flow chart.

changes under different oceanic influences without considering nonlinear interactions across basins. The remaining set uses specified time-varying SST for six designated oceanic regions, with climatological SST input for other ocean basins, to investigate the impact of multi-basin forcing on global SAT in section 3.2 (figure 1). Six key oceanic regions were selected here for simulation, Indian Ocean (IO; 20° S–20° N, 40°–120° E), North Atlantic (NA; 0°–60° N, 0°–80° W), western Pacific (WP; 20° S–20° N, 120° E–180°), eastern tropical Pacific (TP; 10° S–10° N, 90° W–180°), North Pacific (NP; 20°–70° N, 110° E–100° W), and Southern Ocean (SO; 40°–70° S, 0°–360°) (section S2 and Xu *et al* 2020).

2.3. Statistical methods

This study primarily employs statistical methods such as correlation analysis, climate trend analysis, linear regression analysis, and effective degrees of freedom testing. Trend changes in climate sequences are estimated using least squares estimation method. The relationship between regional SST and global SAT time series is verified by calculating standardized anomalies. Correlation coefficients between model-simulated and observed SST indices and global SAT are calculated, with significance tested using a two-tailed *Student's t*-test with effective degrees of freedom (N_{eff}). For variables X and Y, their significance can be approximated as follows (Bretherton *et al* 1999):

$$\frac{1}{N_{\text{eff}}} \approx \frac{1}{N} + \frac{2}{N}\sum_{i=1}^{N}\frac{N-i}{N}\rho_{XX}(i)\,\rho_{YY}(i), \qquad (2\text{–}1)$$

where N is the total sample size of the time series, and $\rho_{XX}(i)$ and $\rho_{YY}(i)$ denote the autocorrelation of two time series X and Y at time lag i, respectively.

3. Results

3.1. The accumulative interdecadal trend of global SAT generated by separate simulations of six ocean basin SSTs

The impact of six selected basin-scale SSTs on global SAT over different time scales are first investigated (figure S1). From 1910 to 1975, the SAT changes under the influence of the six selected basin SSTs closely capture the global historical SST simulated interdecadal trends in SAT. While for 1975–2012, the accumulative global SAT driven by basin-scale SSTs is significantly higher than that generated by global historical SSTs. This suggests that, before the 1970s, the SST primarily modulated global SAT changes through linear effects. In contrast, after 1970, nonlinear effects and other factors within the climate system began to significantly impact SAT.

To further explore the role of SSTs in specified ocean basins on global interdecadal SAT change during different periods, we implement several numerical simulations (section S3 and Xu *et al* 2020). The SSTs exhibit regional and temporal phase-locking characteristics in regulating global SAT. The selected

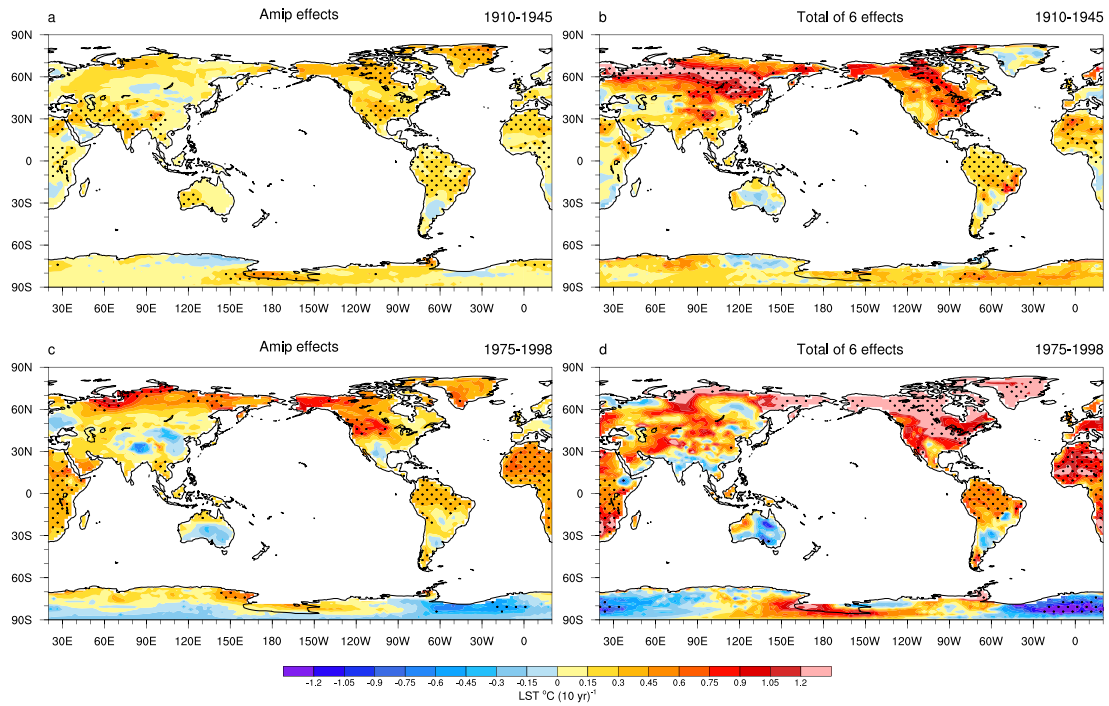

Figure 2. Simulated SAT spatial patterns of the trend for (a), (b) 1910–1945 and (c), (d) 1975–1998. (a), (c) Both show the SAT simulated by historical global SST forcing experiment. (b), (d) Both show the SAT accumulated from the results simulated by the six ocean basins' SSTs forcing experiments. Shading represents SAT trends per decade in °C 10 yr^{-1}. Stippling indicates regions exceeding the 95% confidence level (*Student's t*-test).

six ocean basins' SST forcing experiment can generate global interdecadal SAT changes in 1910–1945 and 1975–1998 accelerated warming periods. While for the other periods, specific ocean basins SSTs play more important role in regulating the global SAT warming slowdown changes compare to the six basin-scale SSTs. During 1940–1975, SSTs in the Indian Ocean, North Atlantic, and western Pacific primarily contributed to the global SAT temporal change. During 1998–2012, the combination of SAT temporal change simulated by eastern tropical Pacific and North Pacific SSTs forcing are consistent with that of global historical SST forcing simulation (figure S2).

The spatial consistency rates of SAT trend between the accumulated six basin-scale SST forcing simulations and historical SST forcing simulation during 1910–1945 and 1975–1998, are 86.6% and 74.8%, respectively (figure 2). The consistency is especially pronounced in low-latitude areas (30° S–30° N). The simulations effectively capture significant warming trends in North America, South America, South Asia, and Africa. These results suggest that SST in the six ocean basins were the dominant driver of the notable global SAT warming during 1910–1945 and 1975–1998. While the accumulated SST forcing from multiple ocean basins notably amplified the impact of external radiative forcing, thereby amplifying the magnitude of global warming. Further studies are required to investigate the magnitude of external forcing's contribution to global warming rate.

For 1940–1975, the accumulative SST forcing simulation results in the Indian Ocean, North Atlantic, and western Pacific accurately capture the spatial distribution and magnitude of the 10 year interdecadal SAT trends of global historical SST forcing simulation in Eurasia, most of west-central North America, South America, Africa, and southern Oceania (figure 3(b)). The spatial sign consistency rate between the two is 64.9%. The result suggests that the combination SST effect of Indian Ocean, North Atlantic, and western Pacific is the primary reason driving the global SAT interdecadal cooling trend observed during 1940–1975.

In 1998–2012, the spatial distribution of land SAT trends resulting from the accumulated SST forcing of the eastern tropical Pacific and North Pacific basins reflects notable warming trends in the high-latitude regions of Eurasia and southern North America. Also accurately reproduce the spatial SAT trend patterns across much of Eurasia, central and western North America, South America, Africa, and Oceania, as well as the seesaw-like SAT pattern along the east and west coasts of mid- and high-latitude North America (figures 3(c) and (d)). Compared to historical SST forcing experiments, the correlation between the two simulations is 68.4%, with a spatial sign consistency rate of 70.7%, which is significantly higher than the spatial sign consistency rate of 60.3% obtained when combining SST forcing simulations from all six basin-scale regions (figure omitted). These findings suggest

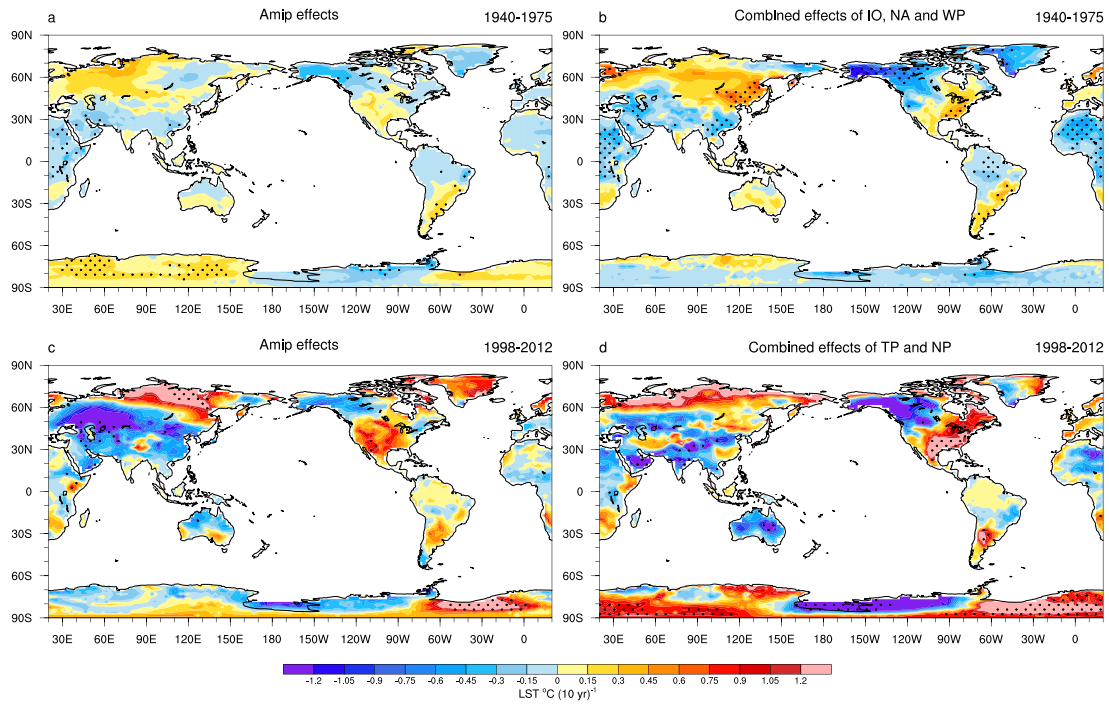

Figure 3. Simulated SAT spatial patterns of the trend for (a), (b) 1940–1975 and (c), (d) 1998–2012. (a), (c) Both show the SAT simulated by historical global SST forcing experiment. (b) Shows the SAT accumulated from the results simulated by the North Atlantic, western Pacific, and Indian Ocean SST forcing simulations. (d) Shows the SAT accumulated by the eastern tropical Pacific and North Pacific SST forcing simulations. Shading represents SAT trends per decade in °C 10 yr^{-1}. Stippling indicates regions exceeding the 95% confidence level (*Student's t*-test).

that the SST in eastern tropical Pacific and North Pacific together dominated the global interdecadal SAT spatiotemporal changes during 1998–2012, especially in the context of the global warming slowdown.

It is important to note that the direct superposition of SST forcing simulations from these six ocean basins amplifies the nonlinear interactions between the regions and the effects of external radiative forcing on the climate system. This leads us to understand the combined impact of SSTs from the select ocean basins on global SAT interdecadal trend.

3.2. The joint contribution of SSTs' co-forcing at multi-ocean-basins to the trend of global SAT

The direct superposition of SST-forced simulations for the selected ocean regions may not reflect the actual internal climate variability and external radiative forcing effect. Discrepancies may arise in SAT changes compared to that generated by global historical SST-forcing simulation due to errors. These errors include repeated calculations for dynamics and physics processes within the climate system, ignoring thermohaline circulation of the ocean. Thus, we conducted a sensitivity experiment. Here, the six key ocean regions were treated as a unified whole, with their historical SSTs serving as the forcing input for the atmospheric lower boundary in the model, while the remaining ocean regions were driven by climatological SSTs. This configuration was used to drive the model and explore the impact of the combined SST forcing from these selected ocean regions on global SAT interdecadal variability.

As shown in figure S3, under the combined SST forcing from the six selected ocean basins, the simulation successfully reproduced the global SAT time series from 1910 to 2012, aligning closely with both the GISS data and global historical SST forcing experiment results. The model accurately captured the interdecadal SAT trends and interannual oscillations during the four periods of interest in this study. Notably, during 1998–2012, the simulation revealed a more pronounced cooling trend in global SAT under the influence of six ocean basins SSTs' forcing, contrasting with the warming slowdown observed in the GISS data. This disparity is likely attributable to the limitations of the existing earth system models in accurately capturing the distinct characteristics of Arctic amplification and its associated warming impacts. Nonetheless, the simulated SAT trends are largely consistent with the historical SST forcing simulation, with a time series correlation of 0.962 between the two. In terms of consistency, the simulations during the first two periods show a higher agreement with the GISS data compared to the latter two periods, suggesting that the influence of nonlinear climate system interactions on global SAT became more pronounced during the latter periods. Overall, the SSTs of the six selected ocean basins are identified

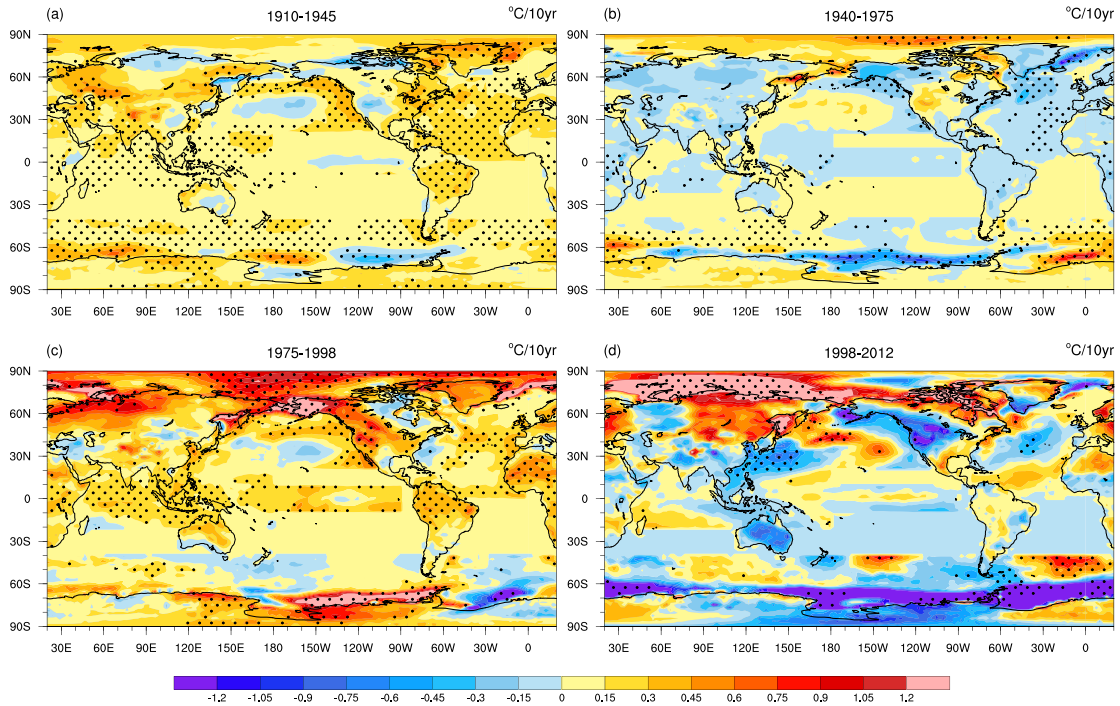

Figure 4. Global SAT spatial trends driven by six ocean basins' SST forcing simulation over four periods. Shading represents the SAT trends for each decade in °C 10 yr^{-1}. Stippling indicates regions exceeding the 95% confidence level (*Student's t*-test).

as the primary drivers of global SAT interdecadal warming slowdown observed between 1910 and 1998.

The SAT trends across the four periods reveals that during the accelerated warming periods, the global warming rate was lower during the 1910–1945 period compared to the 1975–1998 period, with global average SAT warming trends of 0.10 °C 10 yr^{-1} and 0.17 °C 10 yr^{-1}, respectively. In contrast, during the warming slowdown periods, the trend shifted from cooling during 1940–1975 (−0.012 °C 10 yr^{-1}) to a warming slowdown during 1998–2012. Both the model simulations and GISS data indicate that the magnitude of global SAT trend changes increased progressively over time scale from 1910 to 1998, exhibiting a stepwise upward trend.

Further, we explored the influence of the SSTs from the six selected ocean basins on the spatial distribution of global SAT interdecadal trends. The results show that, consistent with the global SAT trends under historical SST forcing, during 1910–1945 and 1975–1998, the global SAT warming trends closely align with those simulated under historical SST forcing (figures 4(a) and (c)). During 1940–1975, the spatial SAT cooling responses across most regions were generally consistent with the global historical SST-forcing results, except for the neglected warming center over Europe (figure 4(b)). During 1998–2012, the SST forcing simulation for the six ocean basins accurately reproduced the spatial distribution of SAT trends across most of North America, high-latitude Eurasia, and Europe, consistent with the historical SST forcing simulation (figure 4(d)). Similar to the time series, the spatial trend patterns during the two accelerated warming periods and the warming slowdown periods also exhibit a pattern where the magnitude of SAT trend changes in the latter period is significantly higher than in the former. These findings indicate that the combinations of SSTs in the six selected ocean basins are key factors that influence the spatial distribution of global SAT interdecadal trends during different periods from 1910 to 2012.

Combined with the significance analysis (stippling in figures 2–4), our results reveal that the influence of SST on interdecadal SAT variations is more stable during periods of accelerated global warming. However, during phases of global warming slowdown, interdecadal SAT variability is influenced by multiple factors, including the long-term warming trend driven by continuous greenhouse gas emissions, external forcings, the significant periodicity of ocean thermohaline circulation changes, and complex nonlinear atmospheric processes. Consequently, the stability of SST's influence on SAT interdecadal variations is lower during warming slowdowns than during accelerated warming periods. Further investigation is required to elucidate the underlying physical mechanisms driving these stability differences.

To quantify the impact of SST forcing from the six ocean basins on regional SAT trends (figure 5), we found that during 1910–1945, Europe experienced a warming center with a rate of 0.24 °C 10 yr^{-1}, slightly higher than the SAT warming trends in other regions, which ranged from 0.08 to 0.16 °C 10 yr^{-1}. In 1975–1998, the warming trend in some regions

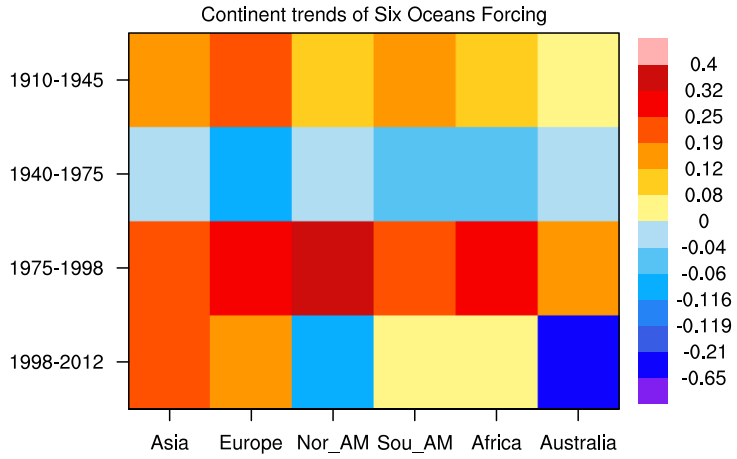

Figure 5. Regional SAT trends driven by six ocean basin SSTs forcing simulation over four periods. Where Nor_AM and Sou_AM represent North America and South America, respectively. Coloring represents the SAT trends for each decade in °C 10 yr^{-1}.

was significantly higher than in the previous warming phase, particularly in North America. Influenced by a strong warming trend along the west coast, North America's warming rate during this period reached 0.37 °C 10 yr^{-1}, more than three times the 0.10 °C 10 yr^{-1} in the region during 1910–1945. This indicates substantial differences in SAT trends within the same region during the two accelerated warming periods. These differences highlight the nonlinear interdecadal growth characteristics of regional SAT.

The SAT trends in different regions during the two warming slowdown periods show significant differences. From 1940 to 1975, the SAT in all regions globally exhibited cooling trends. However, during 1998–2012, significant SAT cooling trends only emerged in North America and Oceania, with trends of −0.1 °C 10 yr^{-1} and −0.36 °C 10 yr^{-1}, respectively. During this period, Eurasia as a whole showed a warming trend of 0.21 °C 10 yr^{-1}, offsetting cooling in other regions. From a regional average perspective, SAT trend changes globally at the regional scale also exhibited a distinct upward phase trend, consistent with the time series.

Comparing the SAT response from historical SST forcing experiment, this study also quantified the relative contribution of SST from the six ocean basins to SAT trends on different continents globally across different periods. During the two accelerated warming periods, SST forcing from the six ocean basins resulted in relatively consistent warming across all continents. In the global cooling period (1940–1975), this forcing led to interdecadal cooling of SAT in North America, South America, and Africa. In addition, the six-region forcing experiment to some extent fixed the exaggeration of interdecadal cooling trends on several continents simulated by the historical SST forcing during the global warming slowdown period (1998–2012). As a result, there were some differences between the two experiments in simulating interdecadal SAT trends. However, the six-region forcing experiment better reflected the SAT spatial trend distribution that is more consistent with observations (figures omitted), especially in North America and Europe (figure S4). Therefore, the SSTs of the six ocean basins are an important internal climate variability driving interdecadal trends in global SAT.

4. Summary and discussion

The interdecadal variability of SAT on global and regional scales is significantly influenced by the combined forcing of SSTs across multiple ocean basins. Without considering nonlinear SST interactions, the combined results from six basin-scale SST forcing experiments suggest that these SSTs generate the overall warming of global SAT during the periods of rapid warming from 1910–1945 and 1975–1998. However, during the periods of 1940–1975 and 1998–2012, the six basin-scale SSTs exhibit significant temporal and regional SST phase-locking characteristics that promote decadal warming slowdowns or even cooling of global SAT. During 1940–1975, the combined effects of the Indian Ocean, North Atlantic, and western Pacific Ocean SST domine the interdecadal spatial and temporal variations in global SAT. From 1998–2012, the combined SST forcing of the equatorial eastern Pacific and North Pacific dominates the generation of global SAT interdecadal spatial and temporal patterns consistent with observations.

The simulation experiment with combined forcing from the six basin SSTs successfully reproduce the interdecadal trends in global SAT as reflected by historical SST forcing. During 1910–1945 and 1975–1998, under the combined influence of the six basin SSTs, SATs across different continents globally exhibit consistent interdecadal warming on a regional average scale. Conversely, during 1940–1975 and 1998–2012, the different continents show spatial patterns of interdecadal cooling and warming slowdown that align with the temporal trends. During

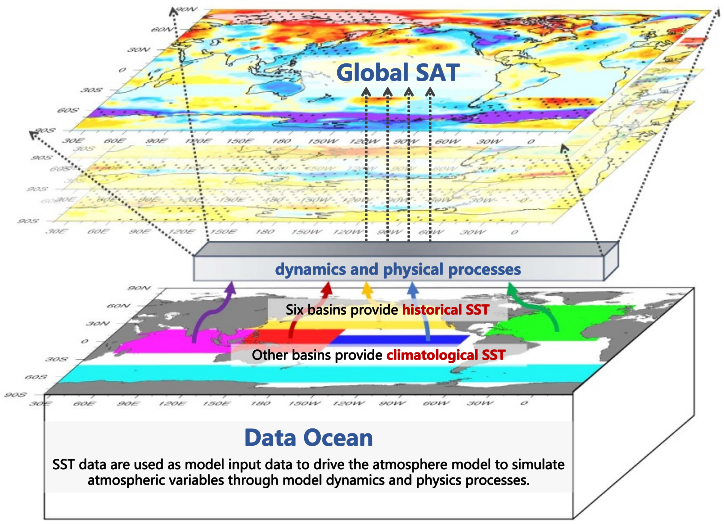

Figure 6. The mechanism diagram. Where red, blue, green, yellow, magenta and cyan boxes represent WP, TP, NA, NP, IO, and SO, respectively.

1940–1975, the global overall SAT interdecadal trend is −0.012 °C 10 yr^{-1}. During 1998–2012, Eurasia exhibits a warming trend. This warming effect offsets the cooling of SATs in regions such as North America and Oceania, shaping the overall global SAT trend pattern. The SAT changes under the six basin SST forcing exhibit high consistency with those under historical SST forcing, indicating that the corresponding basin SSTs are key factors driving global SAT interdecadal variability (figure 6).

Our results demonstrate that interdecadal SAT trends are governed by interactions among SST anomalies across six key ocean basins, mediated by thermodynamic coupling, regional feedbacks, atmospheric teleconnections, and ocean heat redistribution. During rapid warming periods (1910–1945, 1975–1998), concurrent SST warming in the Indian Ocean, western Pacific, and North Atlantic amplified SAT trends through enhanced latent and sensible heat fluxes. For example, Indian Ocean warming intensified convective activity over the Maritime Continent, elevating SAT in adjacent land regions. The weakened AMOC reduced heat transport to high latitudes, leading North Atlantic cooling (1940–1975) and driving SAT declines in Europe (Li *et al* 2013, Chen and Tung 2018). This finding underscores the critical role of inter-basin heat exchange in modulating surface warming. Similarly, cooling in the eastern tropical Pacific (1998–2012) strengthened the Walker Circulation, suppressing convection over the central Pacific while enhancing subsidence over North America. This dynamic response explains the observed SAT cooling in western North America and warming in Eurasia, consistent with La Niña-like teleconnections (Zhang *et al* 1997, Kosaka and Xie 2016). The combined forcing of six basins outperformed the accumulation of individual basin simulations, highlighting the importance of nonlinear synergies. This emphasizes that multi-basin SST effects are not merely additive but dynamically interdependent.

This study, building on prior work, conducts two types of multi-basin SST forcing effect research, systematically quantifying multi-basin SST effects on global and local air temperatures across different periods. The findings strongly support future in-depth investigations into the physical mechanisms of multi-basin scales influencing global climate change. Moreover, they offer a scientific basis for formulating climate change adaptation (such as agricultural planning, water resource management, infrastructure construction) and mitigation strategies (such as marine ecological protection, greenhouse gas emission reduction).

It is worth noting that although our simulation results have well demonstrated the significant role of multi-ocean-basin regions in influencing the interdecadal variations of global air temperature, in the experiments conducted in this paper, SSTs are all presented in the form of data-based SSTs. There are limitations in simulating the regulation of air temperature by air–sea interactions and ocean circulation changes. Therefore, there is still a certain gap between the accuracy of the simulation results and the observations. In addition, the internal climate variability, which affects global SAT interdecadal trends, is also influenced by factors such as the recent Arctic warming effect, air–sea interaction, atmospheric teleconnections (McGregor *et al* 2014, Sun *et al* 2017) and the transfer and storage of energy within the ocean (Meehl *et al* 2012, Chen and Tung 2014). These effects complicate the accuracy of simulations forecasting global SAT interdecadal variability. From a climate dynamics perspective, a deeper understanding of the physical mechanisms within the climate

system is needed. Additionally, regarding the simulations themselves, under the influence of climate change, there is a need to further improve the physical processes and dynamic frameworks of models. Approaches such as combining observations with coupled models and using artificial intelligence to optimize model parameterization schemes require further exploration to enhance the simulation capabilities of numerical models and to delve deeper into the attribution of climate change. It is worth noting that since 2013, global SAT has continued to show an accelerated warming trend. This raises questions about the role of internal climate variability in modulating global SAT, either suppressing or amplifying the warming effects of external radiative forcing. These questions require further in-depth research.

Data availability statement

The GISTEMP data (1910–2017) is openly available at NOAA/OAR/ESRL PSD, Boulder, Colorado, USA. The model simulated data used during this study are openly available from ljp@ouc.edu.cn.

The data that support the findings of this study are openly available at the following URL/DOI: https://esrl.noaa.gov/psd/; http://lijianping.cn/dct/page/65540.

Acknowledgment

This work was supported by the Laoshan Laboratory (No. LSKJ202202600), National Natural Science Foundation of China (NSFC) Project (42130607), Shandong Natural Science Foundation Project (ZR2019ZD12) and Fundamental Research Funds for the Central Universities (202242001). We are grateful to Center for High Performance Computing and System Simulation, Pilot National Laboratory for Marine Science and Technology (Qingdao) for providing computing resource, and NOAA/OAR/ESRL PSD, Boulder, Colorado, USA, which Web site is www.esrl.noaa.gov/psd/ for providing GISTEMP data (1910–2017).

Conflict of interest

The authors declare no competing interests.

Code availability

All the codes that contribute to the data preparation, simulation output analysis, and statistical analysis will be provided by the corresponding author upon reasonable request.

ORCID iDs

Yidan Xu https://orcid.org/0000-0002-5948-4607
Jianping Li https://orcid.org/0000-0003-0625-1575
Jiaxu Guo https://orcid.org/0000-0001-8348-9283

References

Auffhammer M and Mansur E T 2014 Measuring climatic impacts on energy consumption: a review of the empirical literature *Energy Econ.* **46** 522–30
Bretherton C S, Widmann M, Dymnikov V P, Wallace J M and Bladé I 1999 The effective number of spatial degrees of freedom of a time-varying field *J. Clim.* **12** 1990–2009
Chen X Y and Tung K K 2014 Varying planetary heat sink led to global–warming slowdown and acceleration *Science* **345** 897–903
Chen X Y and Tung K K 2018 Global surface warming enhanced by weak Atlantic overturning circulation *Nature* **559** 387–91
Clement A and DiNezio P 2014 The tropical Pacific Ocean—Back in the driver's seat? *Science* **343** 976–8
Dai A 2013 Increasing drought under global warming in observations and models *Nat. Clim. Change* **3** 52–58
Dai A, Fyfe J C, Xie S P and Dai X 2015 Decadal modulation of global surface temperature by internal climate variability *Nat. Clim. Change* **5** 555–9
Deser C, Alexander M A, Xie S P and Phillips A S 2010 Sea surface temperature variability: patterns and mechanisms *Annu. Rev. Mar. Sci.* **2** 115–43
Diffenbaugh N S, Singh D, Mankin J S, Horton D E, Swain D L and Touma D 2017 Quantifying the influence of global warming on unprecedented extreme climate events *Proc. Natl Acad. Sci. USA* **114** 4881–6
England M H, McGregor S, Spence P, Meehl G A, Timmermann A, Cai W, Gupta A S, McPhaden M J, Purich A and Santoso A 2014 Recent intensification of wind–driven circulation in the Pacific and the ongoing warming hiatus *Nat. Clim. Change* **4** 222–7
Fyfe J C and Gillett N P 2014 Recent observed and simulated warming *Nat. Clim. Change* **4** 150–1
Gasparrini A *et al* 2015 Mortality risk attributable to high and low ambient temperature: a multicountry observational study *Lancet* **386** 369–75
Hansen J, Ruedy R, Sato M and Lo K 2010 Global surface temperature change *Rev. Geophys.* **48** RG4004
Huang B Y, Thorne P, Banzon V, Boyer T, Chepurin G, Lawrimore J, Menne M, Smith T, Vose R and Zhang H 2017 Extended reconstructed sea surface temperature, version 5 (ERSSTv5): upgrades, validations, and intercomparisons *J. Clim.* **30** 8179–205
Hurrell J W *et al* 2013 The community earth system model: a framework for collaborative research *Bull. Am. Meteorol. Soc.* **94** 1339–60
Keenlyside N S, Latif M, Jungclaus J, Kornblueh L and Roeckner E 2008 Advancing decadal–scale climate prediction in the North Atlantic sector *Nature* **453** 84–88
Kosaka Y and Xie S P 2013 Recent global–warming hiatus tied to equatorial Pacific surface cooling *Nature* **501** 403–7
Kosaka Y and Xie S P 2016 The tropical Pacific as a key pacemaker of the variable rates of global warming *Nat. Geosci.* **9** 669–73
Lean J L and Rind D H 2009 How will earth's surface temperature change in future decades? *Geophys. Res. Lett.* **36** L15708
Li J P, Sun C and Ding R Q 2018 Decadal coupled ocean–atmosphere interaction in North Atlantic and global warming hiatus *Special Publications of the International Union of Geodesy and Geophysics* (Cambridge University Press)
Li J P, Sun C and Jin F-F 2013 NAO implicated as a predictor of Northern Hemisphere mean temperature multidecadal variability *Geophys. Res. Lett.* **40** 5497–502

Li X C, Xie S P, Gille S T and Yoo C 2016 Atlantic–induced pan–tropical climate change over the past three decades *Nat. Clim. Change* **6** 275–9
Lobell D B, Schlenker W and Costa-Roberts J 2011 Climate trends and global crop production since 1980 *Science* **333** 616–20
McGregor S, Timmermann A, Stuecker M F, England M H, Merrifield M, Jin F-F and Chikamoto Y 2014 Recent Walker circulation strengthening and Pacific cooling amplified by Atlantic warming *Nat. Clim. Change* **4** 888–92
Meehl G A *et al* 2012 Climate system response to external forcings and climate change projections in CCSM4 *J. Clim.* **25** 3661–83
Meehl G A, Arblaster J M, Fasullo J T, Hu A and Trenberth K E 2011 Model–based evidence of deep–ocean heat uptake during surface–temperature hiatus periods *Nat. Clim. Change* **1** 360–4
Merrifield M A, Thompson P R and Lander M 2012 Multidecadal sea level anomalies and trends in the western tropical Pacific *Geophys. Res. Lett.* **39** 34–47
Mochizuki T, Kimoto M, Watanabe M, Chikamoto Y and Ishii M 2016 Interbasin effects of the Indian Ocean on Pacific decadal climate change *Geophys. Res. Lett.* **43** 7168–75
Nidheesh A G, Lengaigne M, Vialard J, Unnikrishnan A S and Dayan H 2013 Decadal and long–term sea level variability in the tropical Indo–Pacific Ocean *Clim. Dyn.* **41** 381–402
Nie G, Yang J, Zhang Y, Xiao X, Xia J C, Cai X and Li C 2024 Duration of exposure to compound daytime-nighttime high temperatures and changes in population exposure in China under global warming *Hum. Soc. Sci. Commun.* **11** 1–12
Nieves V, Willis J K and Patzert W C 2015 Recent hiatus caused by decadal shift in Indo–Pacific heating *Science* **349** 532–5
Rayner N A, Parker D, Horton E, Folland C, Alexander L, Rowell D, Kent E and Kaplan A 2003 Global analyses of sea surface temperature, sea ice, and night marine air temperature since the late Nineteenth Century *J. Geophys. Res. Atmos.* **108** D14
Screen J A and Simmonds I 2010 The central role of diminishing sea ice in recent Arctic temperature amplification *Nature* **464** 1334–7
Sun C, Kucharski F, Li J P, Jin F-F, Kang I S and Ding R 2017 Western tropical Pacific multidecadal variability forced by the Atlantic multidecadal oscillation *Nat. Commun.* **8** 15998
Sun C, Li J and Jin F-F 2015 A delayed oscillator model for the quasi–periodic multidecadal variability of the NAO *Clim. Dyn.* **45** 2083–99
Tan H, Cai R, Yan X and Li C 2021 Amplification of winter sea surface temperature response over east China seas to global warming acceleration and slowdown *Int. J. Climatol.* **41** 2082–99
Timmermann A, McGregor S and Jin F-F 2010 Wind effects on past and future regional sea level trends in the southern Indo–Pacific *J. Clim.* **23** 4429–37
Trenberth K E 2015 Has there been a hiatus? *Science* **349** 691–2
Trenberth K E and Fasullo J T 2013 An apparent hiatus in global warming? *Earth's Future* **1** 19–32
Xie S P and Kosaka Y 2017 What caused the global surface warming hiatus of 1998–2013? *Curr. Clim. Change Rep.* **3** 128–40
Xu Y D *et al* 2020 Contribution of SST change to multidecadal global and continental surface air temperature trends between 1910 and 2013 *Clim. Dyn.* **54** 1295–313
Xu Y D, Li J P and Fu H H 2022 The role of sea surface temperature variability in changes to global surface air temperature related to two periods of warming slowdown since 1940 *Clim. Dyn.* **59** 499–517
Yu W, Yang J, Sun D, Ren J, Xue B, Sun W, Xiao X, Xia J and Li X 2024 How urban heat island magnifies hot day exposure: global unevenness derived from differences in built landscape *Sci. Total Environ.* **945** 174043
Zhang M, Chen E, Zhang C and Han Y 2024a Impact of seasonal global land surface temperature (LST) change on gross primary production (GPP) in the early 21st century *Sustain. Cities Soc.* **110** 105572
Zhang M, Yiğit I, Adıgüzel F, Hu C, Chen E, Siyavuş A E, Elmastaş N, Ustuner M and Kaya A Y 2024b Impact of urban surfaces on microclimatic conditions and thermal comfort in Burdur, Türkiye *Atmosphere* **15** 1375
Zhang Y, Wallace J M and Battisti D S 1997 ENSO–like interdecadal variability: 1900–93 *J. Clim.* **10** 1004–20